Developmental Cell
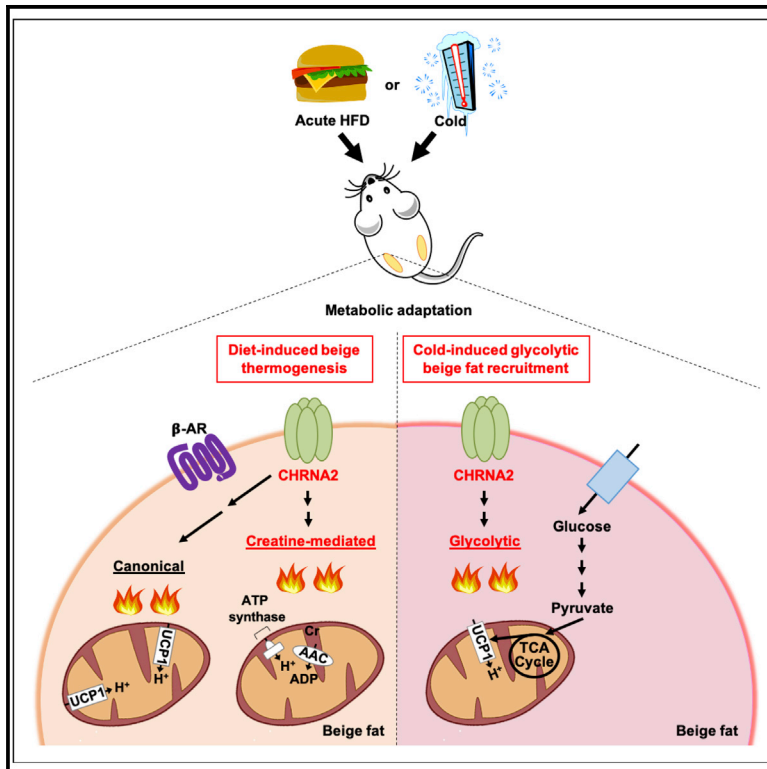
Adrenergic-Independent Signaling via CHRNA2 Regulates Beige Fat Activation

Graphical Abstract

Highlights

- CHRNA2 signaling in adipocytes mediates systemic energy homeostasis *in vivo*

- Acute high fat diet feeding activates CHRNA2 signaling in beige adipocytes

- CHRNA2 signaling regulates both UCP1- and creatine-mediated pathways

- CHRNA2 signaling regulates the activation of glycolytic beige adipocytes

Authors

Heejin Jun, Yingxu Ma, Yong Chen, ...,
X.Z. Shawn Xu,
Shingo Kajimura, Jun Wu

Correspondence

wujunz@umich.edu

In Brief

Jun et al. show that adipocyte-autonomous CHRNA2 signaling mediates adaptive thermogenesis after cold exposure and metabolic homeostasis during high fat diet feeding. Upon activation after acute calorie excess, CHRNA2 signaling regulates both UCP1- and creatine-mediated pathways. CHRNA2-glycolytic beige adipocytes axis regulates a β-adrenergic-independent signaling pathway.

CellPress

Developmental Cell

CellPress

Article

Adrenergic-Independent Signaling via CHRNA2 Regulates Beige Fat Activation

Heejin Jun,[1,9] Yingxu Ma,[1,3,9] Yong Chen,[4,5,6,10] Jianke Gong,[1,8] Shanshan Liu,[1] Jine Wang,[1] Alexander J. Knights,[1] Xiaona Qiao,[1,7] Margo P. Emont,[1,2] X.Z. Shawn Xu,[1,2] Shingo Kajimura,[4,5,6] and Jun Wu[1,2,11,*]

[1]Life Sciences Institute, University of Michigan, Ann Arbor, MI 48109, USA
[2]Department of Molecular & Integrative Physiology, University of Michigan Medical School, Ann Arbor, MI 48109, USA
[3]Department of Cardiology, the Second Xiangya Hospital, Central South University, Changsha, Hunan 410013, China
[4]UCSF Diabetes Center, San Francisco, CA, USA
[5]Eli and Edythe Broad Center of Regeneration Medicine and Stem Cell Research, San Francisco, CA, USA
[6]Department of Cell and Tissue Biology, University of California, San Francisco, San Francisco, CA, USA
[7]Huashan Hospital, Fudan University, Shanghai 200040, China
[8]International Research Center for Sensory Biology and Technology of MOST, Key Laboratory of Molecular Biophysics of MOE, and College of Life Sciences and Technology, and Huazhong University of Science and Technology, Wuhan, Hubei 430074, China
[9]These authors contributed equally
[10]Present address: Department of Endocrinology, Internal Medicine, Tongji Hospital, Tongji Medical College, Huazhong University of Science and Technology, Wuhan, China
[11]Lead Contact
*Correspondence: wujunz@umich.edu
https://doi.org/10.1016/j.devcel.2020.05.017

SUMMARY

Maintaining energy homeostasis upon environmental challenges, such as cold or excess calorie intake, is essential to the fitness and survival of mammals. Drug discovery efforts targeting β-adrenergic signaling have not been fruitful after decades of intensive research. We recently identified a new beige fat regulatory pathway mediated via the nicotinic acetylcholine receptor subunit CHRNA2. Here, we generated fat-specific *Chrna*2 KO mice and observed thermogenic defects in cold and metabolic dysfunction upon dietary challenges caused by adipocyte-autonomous regulation *in vivo*. We found that CHRNA2 signaling is activated after acute high fat diet feeding and this effect is manifested through both UCP1- and creatine-mediated mechanisms. Furthermore, our data suggested that CHRNA2 signaling may activate glycolytic beige fat, a subpopulation of beige adipocytes mediated by GABPα emerging in the absence of β-adrenergic signaling. These findings reveal the biological significance of the CHRNA2 pathway in beige fat biogenesis and energy homeostasis.

INTRODUCTION

Obesity and related metabolic disorders remain a serious global health concern that is showing no signs of easing. The discovery of thermogenic adipocytes in humans has provided us with new avenues for improving metabolic health; however, our understanding of the pathways and mechanisms that underlie fat thermogenesis is still in its infancy (Chondronikola and Sidossis, 2019; Marlatt and Ravussin, 2017).

It has been well illustrated that thermogenesis operates through the activation of β-adrenergic receptor (β-AR) signaling in response to environmental cues such as cold exposure and caloric excess (Cannon and Nedergaard, 2004; Collins, 2011). Whilst UCP1 has traditionally been regarded as the best-characterized regulator of non-shivering adaptive thermogenesis, several UCP1-independent pathways have come to light in recent years, including futile creatine metabolism (Bertholet et al., 2017; Kazak et al., 2015) and calcium cycling (Ikeda et al.,

2017). Furthermore, the recent demonstration that glycolytic beige (g-beige) fat can emerge during thermal stress in the absence of β-AR signaling indicates the existence of heterogeneous populations of beige adipocytes and thermogenic mechanisms that operate independently of classical signaling pathways (Chen et al., 2019). However, it remains unknown how these newly discovered pathways are integrated during the acclimation to diverse environmental changes, such as nutritional and temperature changes.

Signaling via the nicotinic acetylcholine receptor subunit CHRNA2 was recently identified as a thermogenic pathway selective to beige adipocytes in mice and humans (Jun et al., 2018). Here, we show distinct subcutaneous thermogenic defects in the fat-specific absence of CHRNA2, suggesting a role for CHRNA2-mediated signaling in the orchestration of energy homeostasis following environmental challenges. Thermogenic gene expression and mitochondrial metabolism were impaired in CHRNA2-deficient inguinal fat during chronic cold exposure,
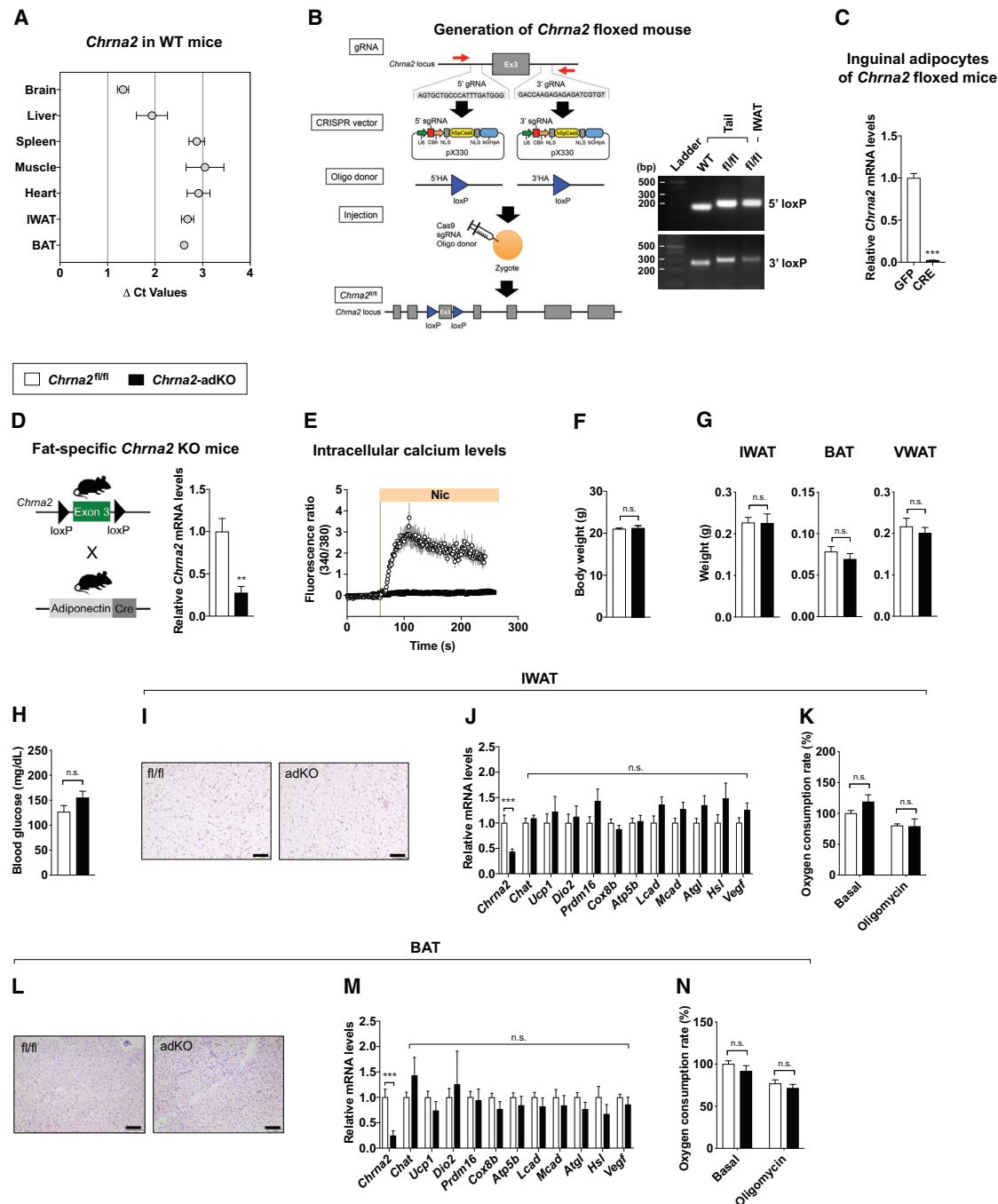
Figure 1. Disruption of CHRNA2 Signaling in Adipose Tissue

(A) qPCR analyses of *Chrna2* mRNA expression across tissues from WT mice (ΔCt relative to *Tbp*, n = 4).

(B) Generation of floxed mice for the conditional deletion of the *Chrna2* gene using the CRISPR/Cas9 system. Exon 3 of the *Chrna2* gene was targeted by sgRNAs designed complementary to intronic sequences flanking the exon, then LoxP sites with a 5′ and 3′ HA were introduced by DNA donor oligonucleotides. The generated sgRNAs, donor oligos, and Cas9 mRNA targeting *Chrna2* were co-injected into zygotes (left). PCR analyses of floxed alleles at the targeted *Chrna2* locus in genomic DNA extracted from the tails and IWAT of WT and *Chrna2*^fl/fl mice (right).

(C) qPCR analyses of *Chrna2* mRNA expression in differentiated primary inguinal preadipocytes of *Chrna2*^fl/fl mice after transduction with adenoviral GFP or Cre recombinase (n = 6).

(D) Breeding strategy for the generation of adipose-specific *Chrna2* knockout mice (*Chrna2*-adKO) (left). qPCR analyses of *Chrna2* mRNA expression in IWAT from *Chrna2*^fl/fl and *Chrna2*-adKO mice (n = 8 for fl/fl and 4 for adKO) (right).

(E) Intracellular calcium levels following stimulation with the CHRNA2 agonist nicotine (Nic, 500 μM) in differentiated primary inguinal preadipocytes from *Chrna2*^fl/fl (n = 8) and *Chrna2*-adKO mice (n = 11).

(legend continued on next page)

Developmental Cell
Article

CellPress

and less protection against high fat diet (HFD) feeding was observed in fat-specific *Chrna2* knockout (KO) mice, whereas no obvious defects were observed at basal level. Following an acute caloric overload that triggers diet-induced thermogenesis (DIT) (Bachman et al., 2002; de Jonge and Bray, 1997; Kazak et al., 2017; Leibel et al., 1995), we found that CHRNA2 signaling mediates DIT in subcutaneous fat through both UCP1- and creatine-dependent pathways. CHRNA2-mediated signaling operates independently of the sympathetic pathway, therefore we investigated whether CHRNA2 plays a role in g-beige fat, a population that is recruited in the absence of β-adrenergic signaling. We cold-challenged mice that had pharmacological or genetic ablation of β-adrenergic signaling and found that *Chrna2* was enriched in GABPα-mediated g-beige fat and elicited the thermogenic program in g-beige fat. Together, our results suggest that CHRNA2 signaling integrates environmental cues to orchestrate a diverse suite of thermogenic pathways in beige fat. The crosstalk between CHRNA2 signaling and g-beige fat activation may suggest innovative therapeutic targets to activate thermogenic fat in humans that may circumvent undesirable side effects associated with β-adrenergic activation.

RESULTS AND DISCUSSION

Disruption of CHRNA2 Signaling in Adipose Tissue

Whole-body *Chrna2* KO mice show distinct thermogenic defects and exacerbated diet-induced obesity (Jun et al., 2018). Given that *Chrna2* is expressed in various tissues including liver, fat, and the brain (Figure 1A), we used CRISPR/Cas9 gene editing to generate a floxed *Chrna2* (*Chrna2*^{fl/fl}) mouse, allowing for tissue-specific *Chrna2* ablation. LoxP sites flanking exon 3 of *Chrna2* were introduced by homology-directed repair and the *in vivo* presence of the inserted LoxP sites on the targeting region was confirmed by genotyping PCR (Figure 1B). Deletion of *Chrna2* by adenoviral delivery of Cre recombinase was confirmed in differentiated *Chrna2*^{fl/fl}-derived inguinal preadipocytes, demonstrating that the LoxP sites appropriately targeted to the endogenous *Chrna2* locus as designed (Figure 1C). To study the effects of *Chrna2* deletion specifically in adipocytes, we generated adipose-specific *Chrna2* KO mice (*Chrna2*-adKO) by crossing *Chrna2*^{fl/fl} animals with *Adiponectin-Cre* mice (Figure 1D). *Chrna2* deletion was confirmed by qPCR in inguinal white adipose tissue (IWAT), with no deletion evident in other tissues that express *Chrna2*, in contrast to the whole-body *Chrna2* KO (Figures 1D and S1A–S1C). Additionally, no other genes encoding nicotinic acetylcholine receptor (nAChR) subunits were induced to compensate for the loss of *Chrna2* expression in IWAT (Figure S1D). We have previously shown that CHRNA2 forms a functional ion channel that can be activated in beige adipocytes in response to its agonists (Jun

et al., 2018). Here, we demonstrated that both nicotine and acetylcholine induced an increase in intracellular calcium in *Chrna2*^{fl/fl}-derived primary inguinal fat cells, indicating that the inserted LoxP sites did not interfere with the production of functional CHRNA2 protein. No response to either agonist was detected in *Chrna2*-adKO cells, demonstrating an effective ablation of CHRNA2 signaling through Cre-mediated deletion in adipocytes (Figures 1E, S1E, and S1F). Similar to what was observed in whole-body *Chrna2* KO animals, fat-specific deletion of *Chrna2* did not cause gross abnormality at the basal condition. *Chrna2*-adKO mice showed no differences in body weight, adipose tissue mass, blood glucose levels, or core body temperature compared to littermate *Chrna2*^{fl/fl} controls (Figures 1F–1H and S1G). Likewise, no morphological differences in IWAT, brown adipose tissue (BAT), or visceral white adipose tissue (VWAT) architecture were seen by hematoxylin and eosin (H&E) staining between the two genotypes, nor did *Chrna2*-adKO mice exhibit any changes in thermogenesis and related glucose metabolism gene expression and oxygen consumption rate (OCR) in IWAT, as well as other key metabolic organs such as BAT, VWAT, and skeletal muscle (Figures 1I–1N and S1H–S1K).

Inguinal Thermogenic Defects by Adipose-Specific *Chrna2* Deletion

This newly generated mouse model with adipose-specific deletion of *Chrna2* now allows us to directly test the hypothesis that the thermogenic defects observed in the IWAT of whole-body *Chrna2* KO mice are mediated through an adipocyte-autonomous mechanism (Jun et al., 2018). We exposed *Chrna2*-adKO and control mice to chronic cold temperature (10°C for 2 weeks) and a blunted weight loss was observed in *Chrna2*-adKO mice compared to that observed in the control group with no differences in food intake (Figures 2A and S2A). This was reflected in their higher fat content, along with their larger IWAT and VWAT mass, although no differences were seen in BAT mass between the two groups, which is consistent with the notion that the functional impact of CHRNA2 signaling is minimal in BAT (Figures 2B and 2C). Histological examination of *Chrna2*-adKO IWAT showed larger adipocytes compared to that of the control mice after cold exposure (Figure 2D). At the transcriptional level, thermogenic genes (*Ucp1*, *Dio2*, *Prdm16*, *Cox8b*, *Atp5b*, *Lcad*, *Mcad*, *Atgl*, *Hsl*, and *Vegf*) were less induced upon chronic cold exposure in *Chrna2*-adKO mice (Figure 2E). Likewise, protein expression of UCP1 and mitochondrial oxidative phosphorylation complexes was significantly less induced in *Chrna2*-adKO IWAT (Figures 2F and 2G). These mice also exhibited less citrate synthase activity and mitochondrial DNA content in IWAT compared to that of the control animals (Figures 2H and S2B). Consistent with these results, whole-body oxygen

(F and G) Body (F) and adipose tissue (G) weights of *Chrna2*^{fl/fl} (n = 8) and *Chrna2*-adKO (n = 4) mice housed at room temperature on a chow diet.

(H) Fasting (4 h) blood glucose levels of *Chrna2*^{fl/fl} (n = 4) and *Chrna2*-adKO (n = 5) mice.

(I–K) Representative H&E-stained images (I), qPCR analyses (n = 14 for fl/fl and 20 for adKO) (J), and basal and oligomycin-insensitive oxygen consumption rate (n = 6) (K) of IWAT from *Chrna2*^{fl/fl} and *Chrna2*-adKO mice. Scale bar, 100 μm.

(L–N) Representative H&E-stained images (L), qPCR analyses (n = 11 for fl/fl and 8 for adKO) (M), and basal and oligomycin-insensitive oxygen consumption rate (n = 6) (N) of BAT from *Chrna2*^{fl/fl} and *Chrna2*-adKO mice. Scale bar, 100 μm.

Data are presented as mean ± SEM. **p < 0.01, ***p < 0.005 by an unpaired two sample Student's t test for two-group comparisons. n.s., not significant (p > 0.1). See also Figure S1.
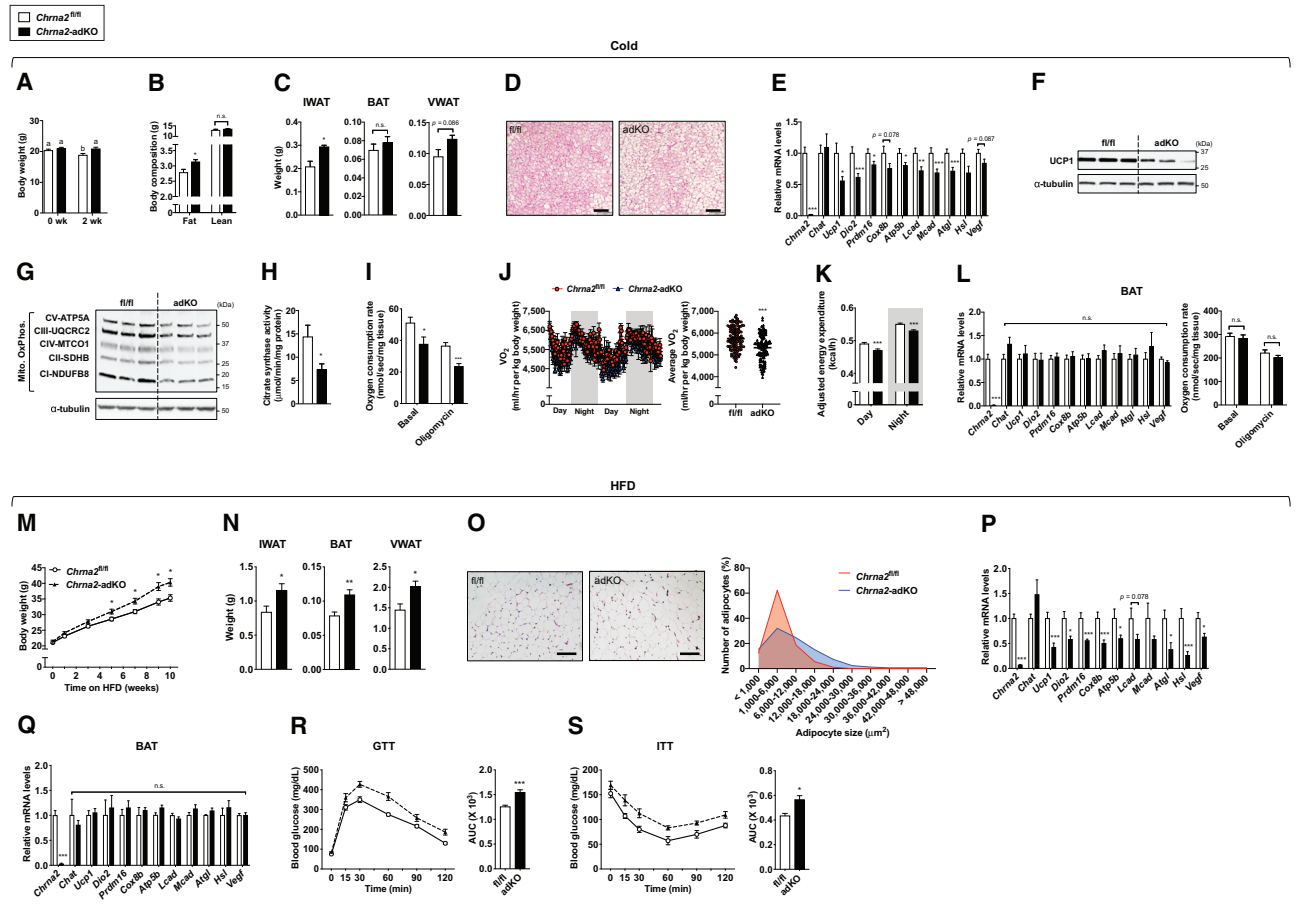
Figure 2. Inguinal Thermogenic Defects by Adipose-Specific *Chrna2* Deletion

(A) Body weights of *Chrna2*^{fl/fl} (n = 19) and *Chrna2*-adKO (n = 18) mice before and after cold exposure (CE) at 10°C for 2 weeks on a chow diet.

(B) Body composition of *Chrna2*^{fl/fl} (n = 6) and *Chrna2*-adKO (n = 6) mice after CE.

(C) Adipose tissue weights of *Chrna2*^{fl/fl} (n = 5) and *Chrna2*-adKO (n = 4) mice after CE.

(D) Representative H&E-stained images of IWAT from *Chrna2*^{fl/fl} and *Chrna2*-adKO mice after CE. Scale bar, 100 μm.

(E) qPCR analyses of thermogenic gene expression in IWAT from *Chrna2*^{fl/fl} (n = 17) and *Chrna2*-adKO (n = 20) mice after CE.

(F and G) Immunoblot analyses of UCP1 (F) and mitochondrial OxPhos components (G) in IWAT from *Chrna2*^{fl/fl} and *Chrna2*-adKO mice after CE (n = 3). α-tubulin served as a loading control.

(H) Citrate synthase activity in homogenates of IWAT from *Chrna2*^{fl/fl} (n = 6) and *Chrna2*-adKO (n = 8) mice following CE.

(I) Basal and oligomycin-insensitive oxygen consumption rate in freshly isolated IWAT from *Chrna2*^{fl/fl} (n = 6) and *Chrna2*-adKO mice (n = 7) after CE.

(J) Whole-body O_2 consumption (VO_2) (left) and averaged VO_2 (right) of *Chrna2*^{fl/fl} (n = 7) and *Chrna2*-adKO (n = 5) mice after CE.

(K) Body weight-adjusted energy expenditure of *Chrna2*^{fl/fl} (n = 7) and *Chrna2*-adKO mice (n = 5) after CE.

(L) qPCR analyses for thermogenic markers (n = 16 for fl/fl and 14 for adKO) (left) and basal and oligomycin-insensitive oxygen consumption rate (n = 6 for fl/fl and 9 for adKO) (right) of BAT from *Chrna2*^{fl/fl} and *Chrna2*-adKO mice following CE.

(M) Changes in body weights of *Chrna2*^{fl/fl} (n = 11) and *Chrna2*-adKO (n = 5) mice upon HFD feeding.

(N) Fat mass of *Chrna2*^{fl/fl} (n = 10) and *Chrna2*-adKO (n = 7) mice after 11 weeks on HFD.

(O) Representative H&E-stained images (left) and distribution of adipocyte size (right) of IWAT from *Chrna2*^{fl/fl} and *Chrna2*-adKO mice after HFD challenge. Scale bar, 100 μm.

(P and Q) qPCR analyses for thermogenic markers of IWAT (P) and BAT (Q) from *Chrna2*^{fl/fl} (n = 5) and *Chrna2*-adKO (n = 7) mice following HFD feeding.

(R and S) Glucose tolerance test (GTT) (R) and insulin tolerance test (ITT) (S) in *Chrna2*^{fl/fl} (n = 5) and *Chrna2*-adKO (n = 7) mice after 9 and 10 weeks on HFD, respectively. AUC, area under the curve.

Data are presented as mean ± SEM. *p < 0.05, **p < 0.01, and ***p < 0.005 by an unpaired two sample Student's t test for two-group comparisons. A different letter means a significant difference among groups at p < 0.05 by a one-way analysis of variance (ANOVA). n.s., not significant (p > 0.1). See also Figure S2.

consumption (VO_2) and energy expenditure as well as the local OCR of IWAT in *Chrna2*-adKO was lower in comparison to control with reduced utilization of both carbohydrate and fat substrates in the absence of *Chrna2* (Figures 2I–2K and S2C–S2E). Additionally, lower glucose metabolism-related thermogenesis in *Chrna2*-adKO mice relative to controls was detected (Figures

S2F and S2G). Given previous findings showing that CHRNA2-mediated thermogenic signaling is beige fat-selective (Jun et al., 2018), it was not surprising that no differences were seen in adipocyte histology or thermogenic responses in either BAT or VWAT from control and *Chrna2*-adKO mice (Figures 2L and S2H–S2L), nor were any significant differences in

shivering-related gene expression observed in the skeletal muscle (Figure S2M). In line with these findings, an impaired molecular thermogenic response to cold was seen in IWAT selectively when CHRNA2 signaling was deleted in *Ucp1*-expressing thermogenic adipocytes by crossing *Chrna2*^fl/fl mice with *Ucp1-Cre* mice (Figures S2N and S2O). Together these results revealed an adipocyte-autonomous mechanism mediated through CHRNA2 that occurs primarily in the subcutaneous fat to control the thermogenic response to chronic cold exposure.

To understand the significance of fat-specific CHRNA2 signaling in systemic metabolic homeostasis, we challenged *Chrna2*^fl/fl and *Chrna2*-adKO mice with HFD. Upon HFD feeding, *Chrna2*-adKO mice showed greater body weight gain than control animals without differences in food intake as a result of higher fat mass in all three major fat depots, IWAT, VWAT, and BAT (Figures 2M, 2N, S2P, and S2Q). Histological and quantitative analyses of inguinal adipocyte size confirmed that *Chrna2*-adKO mice had lower frequency of small-sized adipocyte but higher frequency of large-sized adipocyte compared to controls (Figure 2O). IWAT of HFD-fed *Chrna2*-adKO mice expressed lower levels of thermogenic gene expression than that of controls, whereas this effect was not seen in BAT (Figures 2P and 2Q). HFD feeding caused significantly higher levels of macrophage-related inflammatory and NADPH oxidase-related oxidative stress gene expression in VWAT of *Chrna2*-adKO mice relative to that of control mice (Figure S2R). *Chrna2*-adKO mice showed significantly impaired glucose tolerance and insulin sensitivity compared to control animals, assayed after chronic HFD feeding (Figures 2R and 2S). Together, these data indicate that CHRNA2 signaling in adipocytes plays an important role in systemic energy homeostasis and protects the organism against metabolic stress.

Activation of CHRNA2 Signaling in IWAT during Acute Calorie Overload

Following acute high caloric intake, compensatory increases in energy expenditure are initiated to appropriately restore energy homeostasis via a process, referred to as DIT (Leibel et al., 1995). This phenomenon is mediated, at least in part, by thermogenic fat (Bachman et al., 2002; Hibi et al., 2016; Rothwell and Stock, 1979). UCP1 and β-ARs are well-known molecular mediators that facilitate DIT in fat (Bachman et al., 2002; Feldmann et al., 2009). However, the thermogenic pathways driven by these candidates are not sufficient to explain the mechanism of DIT (Anunciado-Koza et al., 2008; Thomas and Palmiter, 1997). We next investigated how CHRNA2 signaling may respond to metabolic fluctuation following acute excess calorie intake.

Expression of genes encoding catecholamine synthesis machinery (*Th*, *Dbh*, and *Ddc*) and ARs (nine subtypes including *Adra1a*, *Adra1b*, *Adra1d*, *Adra2a*, *Adra2b*, *Adra2c*, *Adrb1*, *Adrb2*, and *Adrb3*; adrenergic thermogenic regulators) was broadly upregulated in the IWAT of wild-type (WT) mice fed a HFD for 3 days, as were levels of *Chrna2* and the acetylcholine synthesis enzyme *Chat* (cholinergic thermogenic regulators) (Figure 3A). This gene activation continued following 10 days of HFD (Figure S3A). Thermogenic activation can occur in unison with or independent of the mitochondrial uncoupling activity of UCP1 in mammalian subcutaneous fat (Ikeda et al., 2017; Kazak

et al., 2015). Creatine has been reported to stimulate ADP-dependent respiration through substrate cycling in *Ucp1*-deleted beige fat (Kazak et al., 2015). A recent study revealed that creatine energetics participates in DIT in murine subcutaneous fat (Kazak et al., 2017, 2019). Thermogenic genes including *Ucp1*, *Prdm16*, and *Cox8b* were upregulated following 3 days of HFD, in addition to mild induction of *Gatm* (creatine biosynthesis) and *Ckmt2* (mitochondrial creatine kinase), hallmarks of thermogenic creatine energetics (Figure 3B).

It has been reported that creatine-dependent thermogenic mechanism plays a predominant role in the absence of UCP1. (Kazak et al., 2015). Therefore, we exposed *Ucp1* KO mice to acute HFD to test whether CHRNA2 signaling plays a role in UCP1-independent thermogenesis. In IWAT of *Ucp1* KO mice, activation of genes for catecholamine synthesis and ARs was seen after acute HFD challenge, as well as *Chat* and *Chrna2* (Figure 3C). This trend was similarly observed in downstream thermogenic genes *Dio2*, *Prdm16*, and *Cox8b*, in addition to creatine metabolism genes, such as *Gamt*, *Gatm* and *Ckmt1* (Figure 3D). We further confirmed that the transcriptional induction of *Chrna2* and downstream thermogenic markers remained evident at thermoneutrality, consistent with previous reports that DIT can be sufficiently activated in the absence of thermal stress (Feldmann et al., 2009; Kazak et al., 2017) (Figure S3B).

We validated that the gene expression pattern of *Chrna2*, its inducibility in response to thermogenic stimuli and its functionality when treated with agonists were all unaffected by the absence of UCP1 in inguinal adipocytes (Figures 3E and S3C–S3E). These allowed us to further investigate the role of CHRNA2 signaling in creatine-mediated beige thermogenesis in an adipocyte-autonomous manner. In differentiated primary inguinal preadipocytes from *Ucp1* KO mice, *Chrna2* and creatine metabolism genes were elevated by nicotine treatment (however, creatine biosynthesis genes *Gamt* and *Gatm* are mildly repressed in the conditions we tested) (Figure 3F), and this was accompanied by an increase in cellular OCR (Figure 3G). However, an induction of nicotine-dependent creatine metabolism gene expression was not seen when *Chrna2* was deleted (Figure 3H). These findings are consistent with results from human primary subcutaneous adipose-derived stromal cells (ASCs), in which expression of *CHRNA2*, *GATM*, *SLC6A8*, and *CKMT2* was activated following nicotine stimulation (Figure 3I). In line with these observations, we found that adipose-specific *Chrna2* deletion indeed caused defects in diet-induced thermogenic response of IWAT with a significantly lower thermogenic gene expression in IWAT than controls after acute HFD feeding (Figure 3J). These effects persisted as HFD challenge continued in fat-specific *Chrna2* KO mice (Figure S3F). Similarly, IWAT of whole-body *Chrna2* KO mice expressed significantly lower thermogenic genes compared to that of control WT mice after prolonged HFD feeding (Figure S3G), leading to impaired whole-body energy expenditure as a metabolic consequence of the accumulative thermogenic defects (Jun et al., 2018). Interestingly, CHRNA2 signaling did not affect SERCA2b-mediated calcium cycling, a separate UCP1-independent thermogenic regulatory pathway (Figures S3H–S3J). This is consistent with the notion that CHRNA2 signaling was mediated via external Ca^{2+} influx (Figure S3K), whereas SERCA2b-mediated calcium cycling is dependent on internal Ca^{2+} release or cycling through
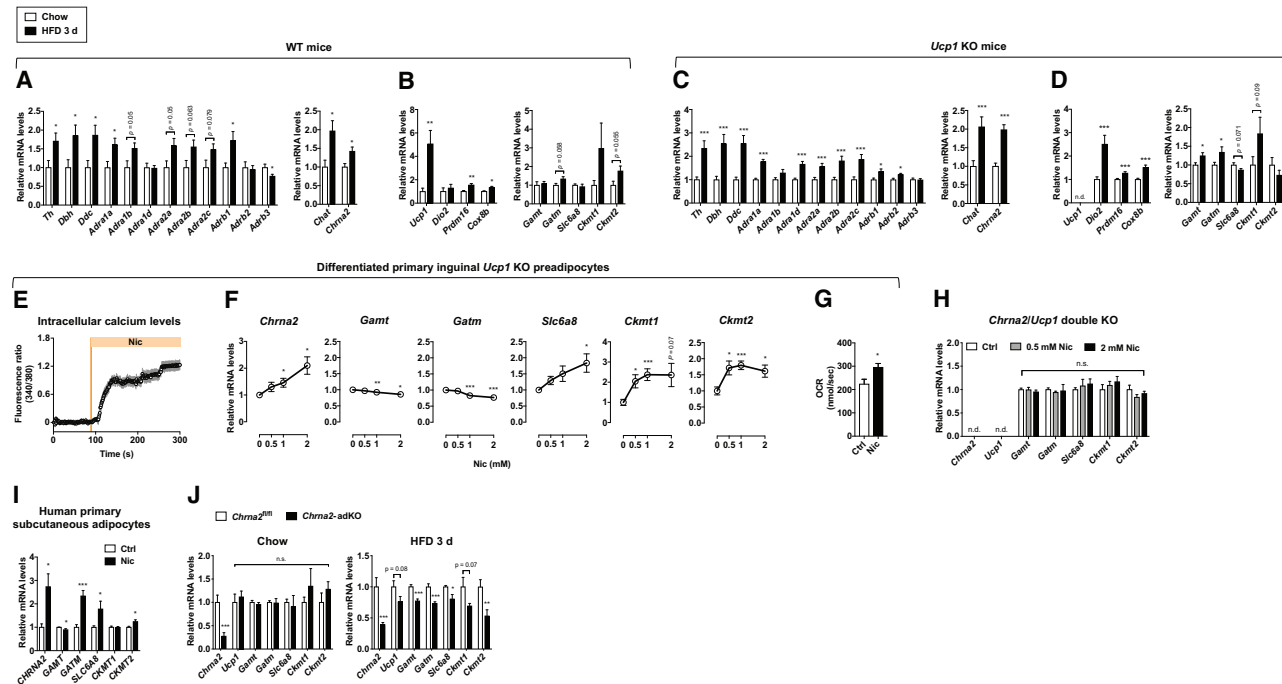
Figure 3. Activation of CHRNA2 Signaling in IWAT during Acute Calorie Overload

(A) qPCR analyses for upstream regulators of thermogenesis (β-AR signaling, left; CHRNA2 signaling, right) in IWAT from WT mice fed chow diet (n = 6) or HFD (n = 7) for 3 days at room temperature (RT).

(B) qPCR analyses for downstream markers of thermogenesis (classical thermogenic markers, left; creatine metabolism-related genes, right) in IWAT from WT mice fed chow diet (n = 6) or HFD (n = 7) for 3 days at RT.

(C and D) qPCR analyses for upstream regulators (C) and downstream markers (D) of thermogenesis in IWAT from *Ucp1* KO mice fed chow diet (n = 30) or HFD (n = 28) for 3 days at RT.

(E) Upregulation of intracellular calcium levels in response to the CHRNA2 agonist nicotine (Nic, 500 μM) in differentiated primary inguinal preadipocytes from *Ucp1* KO mice (n = 11), indicating the presence and activation of CHRNA2 signaling in *Ucp1* KO adipocytes.

(F) qPCR analyses of *Chrna2* and creatine metabolism-related gene expression in differentiated primary inguinal preadipocytes from *Ucp1* KO mice after treatment with the indicated concentration of Nic for 6 h (n = 5 for controls and 6 for 0.5, 1, and 2 mM Nic).

(G) Basal oxygen consumption rate in differentiated primary inguinal preadipocytes from *Ucp1* KO mice that were exposed to vehicle control (Ctrl) or 2 mM Nic for 6 h (n = 6).

(H) qPCR analyses of creatine metabolism-related gene expression in differentiated primary inguinal preadipocytes isolated from *Chrna2*/*Ucp1* double KO mice after stimulation with vehicle (Ctrl) or the indicated concentration of nicotine (Nic) for 6 h (n = 6).

(I) qPCR analyses of *CHRNA2* and creatine metabolism-related gene expression in differentiated human primary ASCs from the subcutaneous depot following stimulation with vehicle (Ctrl) or 2 mM Nic for 6 h (n = 3).

(J) qPCR analyses of *Chrna2*, *Ucp1*, and creatine metabolism-related gene expression in IWAT of *Chrna2*fl/fl and *Chrna2*-adKO mice housed at RT on a chow diet (n = 8 for fl/fl and 4 for adKO) (left) or HFD for 3 days (n = 9) (right).

Data are presented as mean ± SEM. *p < 0.05, **p < 0.01, and ***p < 0.005 by an unpaired two sample Student's t test for two-group comparisons. n.s., not significant (p > 0.1). n.d. not detected. See also Figure S3.

---

the endoplasmic reticulum. These results suggest that the activation of CHRNA2 signaling may integrate UCP1 and creatine pathways to facilitate DIT in subcutaneous fat.

Activation of CHRNA2 Signaling in IWAT in the Absence of β-AR Signaling upon Cold

The recent discovery of a developmentally distinct subtype of thermogenic beige fat cell that relies on enhanced glucose oxidation has further consolidated our understanding of thermogenic mechanisms (Chen et al., 2019). This g-beige fat is particularly relevant in the absence of β-AR signaling and emerges from *Myod*-expressing progenitors through the action of the transcriptional regulator GABPα (Chen et al., 2019). To investigate whether the β-adrenergic-independent CHRNA2 signaling

is involved in g-beige fat function, we pre-treated WT mice with the β-blocker propranolol or vehicle for 5 days at room temperature (RT), then housed these mice at RT or 15°C for a further 5 days with the same treatment. Mice administered with β-blocker exhibited over two-fold higher mRNA expression of *Myod* in inguinal stromal vascular fraction (SVF), indicating that the g-beige fat lineage is being recruited when β-adrenergic signaling is transiently blocked. Furthermore, expression levels of *Chrna2* and g-beige fat metabolic genes were increased in the IWAT of these β-blocker-injected mice after cold exposure without mitochondrial dysfunction (Figures S4A and S4B). The simultaneous activation of CHRNA2 and the g-beige fat program is consistent with our hypothesis that these two β-adrenergic-independent pathways may coordinate with each other in
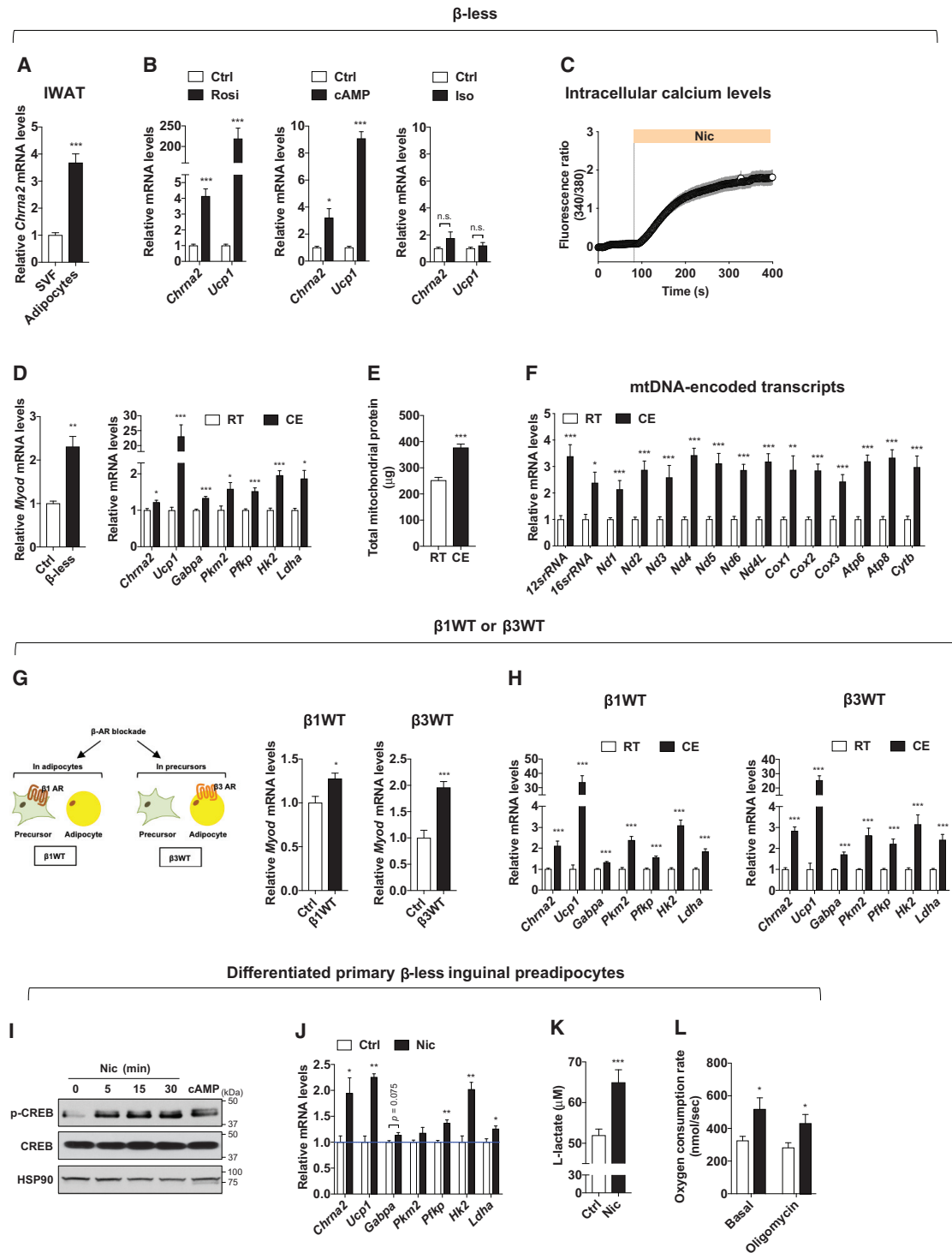
Figure 4. Activation of CHRNA2 Signaling in IWAT in the Absence of β-AR Signaling

(A) qPCR analyses of *Chrna2* mRNA levels in the SVF and mature adipocytes of IWAT from β-less mice housed at RT on a chow diet (n = 6).

(B) qPCR analyses of *Chrna2* and *Ucp1* mRNA levels in differentiated primary inguinal preadipocytes from β-less mice after treatment with vehicle (Ctrl), 1 μM rosiglitazone (Rosi) for 2 days, 500 μM dibutyryl-cAMP (cAMP) for 4 h or 10 μM isoproterenol (Iso) for 4 h (n = 4).

(C) Upregulation of intracellular calcium levels in response to the CHRNA2 agonist nicotine (Nic, 500 μM) in differentiated primary inguinal preadipocytes from β-less mice (n = 24), indicating the presence and activation of CHRNA2 signaling in β-ARs-deleted adipocytes.

(D) qPCR analyses of *Myod* mRNA levels in inguinal SVF of control (Ctrl) and β-less mice (n = 3) (left). qPCR analyses of *Chrna2*, *Ucp1*, and glucose metabolism gene expression in IWAT of β-less mice housed at RT (n = 4) or 15°C (CE) (n = 6) for 5 days (right).

(legend continued on next page)

regulating beige fat function. We further tested this hypothesis using β-less mice, in which β-AR signaling is genetically ablated. In the absence of β-ARs, *Chrna2* expression is enriched in adipocytes and can be induced in response to stimulation with the PPARγ agonist rosiglitazone or second messenger cAMP, similar to what was observed in WT inguinal fat cells (Jun et al., 2018) (Figures 4A and 4B). Following treatment with the pan β-AR agonist isoproterenol, no activation of *Chrna2* and *Ucp1* was observed, confirming the ablation of the β-adrenergic receptors (Figure 4B). Importantly, we confirmed that CHRNA2 forms a functional calcium ion channel that can be activated by its agonists to trigger the downstream pathway in β-ARs KO inguinal adipocytes (Figures 4C and S4C). Similar to what was observed in the pharmacologically blockaded model, *Myod* expression was higher in β-less inguinal SVF compared to that in control counterparts. The co-induction of *Chrna2* and glucose metabolism genes was also observed in the IWAT of cold-exposed β-less animals with enhanced mitochondrial activity and no detectable mitochondrial damages (Figures 4D–4F, S4D, and S4E). It has been reported that the β3-AR predominantly expresses in mature adipocytes whereas β1-AR expression is enriched in preadipocytes (Cannon and Nedergaard, 2004), and the relative contribution of β2-AR signaling in thermogenic fat regulation is minimal in mice (Fernandes et al., 2014). To evaluate the relative contribution of β-adrenergic signaling that occurs at the precursor or mature adipocyte stages in g-beige fat recruitment, we utilized β1WT (β1-AR WT allele was bred back into the β-less background, lacking β2 and β3-AR) and β3WT (β3-AR WT allele was bred back into β-less background, lacking β1 and β2-AR) mouse strains (Figure S4F). We found that the partial blockage of β-adrenergic signaling in these mice was still sufficient to activate the g-beige program to some extent (Figures 4G and 4H). However, only a modest *Myod* induction was observed in β1WT, consistent with the notion that g-beige cell fate determination largely occurs at the precursor recruitment phase. We further tested whether the activated CHRNA2 signaling indeed mediates g-beige fat function in a cell-autonomous manner in differentiated primary inguinal preadipocytes from β-less mice. In the presence of nicotine, CREB was phosphorylated, and the expression of *Ucp1* was elevated in these cells (Figures 4I and 4J), consistent with our previous observations (Jun et al., 2018). Nicotine stimulation also led to an increase in glucose metabolism gene expression and at the functional level, both the abundance of lactate, a product of glycolysis, and the OCR were elevated when CHRNA2 signaling was

activated by its agonist nicotine in β-less inguinal adipocytes (Figures 4J–4L). These data suggest that CHRNA2 signaling may directly activate g-beige fat. It is of note that animal studies showed the recruitment of g-beige fat was significantly blunted in IWAT of *Chrna2* KO mice compared to that of control mice upon cold but not completely absent (Figures S5A–S5C), implicating that additional unknown regulatory pathway(s) may be involved in g-beige fat formation *in vivo*. Detailed understanding of how these pathways interact with each other will continue to evolve as more mechanistic insights of each signaling pathway and new ones are revealed.

The Role of CHRNA2 in Glycolytic Beige Fat Recruitment

We have previously demonstrated that CHRNA2 signaling is activated during canonical beige fat activation in the presence of β-adrenergic signaling (Jun et al., 2018). To investigate how *Chrna2* is activated in non-canonical g-beige fat, we directly tested whether the key regulator of g-beige fat, GABPα may be involved (Figure 5A). Because g-beige fat originates from *Myod*+ progenitors in subcutaneous fat, we first tested whether this specific subpopulation of beige adipocytes indeed has a functional CHRNA2 signaling using calcium imaging assay. Intracellular calcium levels were significantly induced in response to the CHRNA2 agonist nicotine or acetylcholine in *Myod*+-derived g-beige adipocytes, indicating the activation of functional CHRNA2 signaling (Figure 5B). However, when we knocked down *Gabpa* in *Myod*+-derived g-beige adipocytes, *Chrna2* was markedly suppressed relative to controls, strongly suggesting the potential role of CHRNA2 in GABPα-mediated g-beige fat recruitment (Figure 5C).

Next, we used *Gabpa*-expressing C2C12 myoblasts, which under pro-adipogenic conditions can differentiate into g-beige fat (Chen et al., 2019), to examine how CHRNA2 signaling affects the function of g-beige adipocytes. *Chrna2* was enriched in differentiated C2C12 myoblasts expressing *Gabpa* under pro-adipogenic conditions, and it was further induced in response to thermogenic stimuli, such as cAMP and rosiglitazone, along with increased *Ucp1* and glucose metabolism gene expression (Figures 5D, 5E, and S5D). A functional CHRNA2 signaling was detected upon stimulation with its agonist nicotine or acetylcholine in these cells, assessed using calcium imaging assay (Figure S5E). Increased phosphorylated protein kinase A (PKA) substrate and cAMP response element binding protein (CREB), induced glucose metabolism gene expression, as well as *Ucp1* in the presence of nicotine were observed in these *Gabpa*-

(E) Total mitochondrial protein mass of IWAT per mouse from β-less mice housed at RT (n = 8) or CE (n = 10).

(F) qPCR analyses of mitochondrial DNA-encoded transcripts in IWAT from β-less mice housed at RT or CE (n = 6).

(G) Mouse models for genetic deletion of β-AR signaling at the adipocyte (β1WT) or precursor (β3WT) level in IWAT (left). qPCR analyses of *Myod* mRNA levels in inguinal SVF of control, β1WT (n = 6 for Ctrl and 8 for β1WT) (middle) and β3WT (n = 7 for Ctrl and 4 for β3WT) (right) housed at RT.

(H) qPCR analyses of *Chrna2*, *Ucp1*, and glucose metabolism gene expression in IWAT of β1WT (n = 16 for RT and 20 for CE) (left) and β3WT (n = 14 for RT and 16 for CE) (right) mice housed at RT or CE.

(I) Immunoblot analyses for phosphorylation of CREB in differentiated primary inguinal preadipocytes isolated from β-less mice in the presence of 2 mM Nic for indicated time or 500 μM dibutyryl-cAMP (cAMP) for 15 min. HSP90 served as a loading control.

(J) qPCR analyses of *Chrna2*, *Ucp1*, and glucose metabolism gene expression in differentiated primary inguinal β-less preadipocytes that were stimulated with vehicle (Ctrl) or 2 mM Nic for 6 h (n = 3).

(K and L) Intracellular L-lactate levels (n = 20) (K) and basal and oligomycin-insensitive oxygen consumption rate (n = 6 for Ctrl and 5 for Nic) (L) in differentiated primary inguinal β-less preadipocytes following treatments with vehicle (Ctrl) or 2 mM Nic for 6 h.

Data are presented as mean ± SEM. *p < 0.05, **p < 0.01, and ***p < 0.005 by an unpaired two sample Student's t test for two-group comparisons. n.s., not significant (p > 0.1). See also Figure S4.
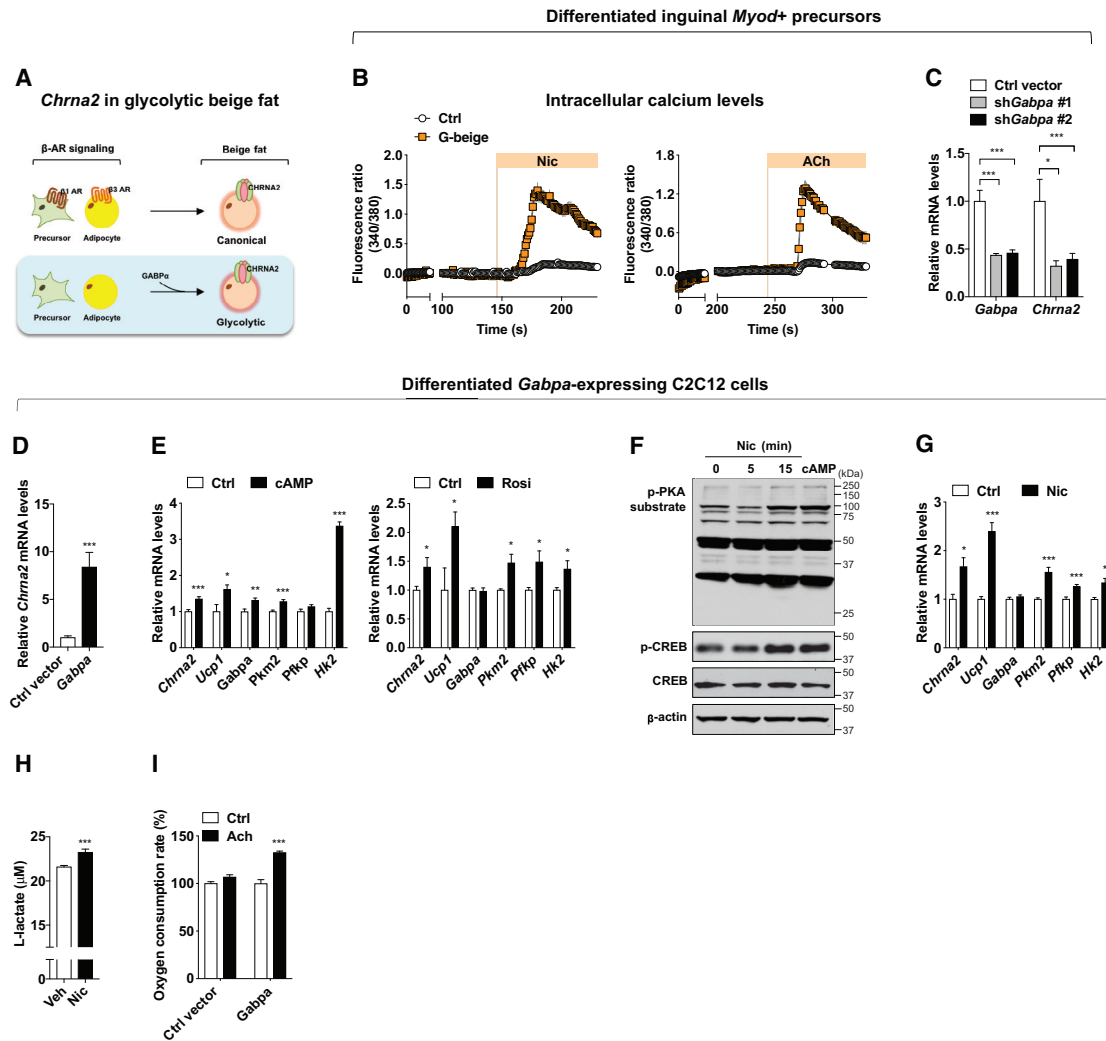
Developmental Cell
Article

CellPress

Figure 5. The Role of CHRNA2 in G-Beige Fat Recruitment

(A) The hypothesis that *Chrna2* is induced during g-beige fat recruitment mediated by GABPα.

(B) Increased intracellular calcium levels in the presence of the CHRNA2 agonist nicotine (Nic, 500 μM) (n = 12) or acetylcholine (ACh, 100 μM) (n = 6) in differentiated *Myod+*-derived g-beige adipocytes. No responses in non-differentiated control cells to the agonists (n = 13 for Nic and 16 for ACh).

(C) qPCR analyses of *Gabpa* (n = 7 for empty vector and 6 for shRNA) and *Chrna2* (n = 5) in *Myod+*-derived glycolytic beige adipocytes expressing empty vector or *Gabpa* shRNA.

(D) qPCR analyses of *Chrna2* mRNA levels in differentiated C2C12 cells expressing empty vector or *Gabpa* under pro-adipogenic conditions (n = 8).

(E) qPCR analyses of *Chrna2*, *Ucp1*, and glucose metabolism gene expression in differentiated C2C12 cells expressing *Gabpa* following stimulation with vehicle (Ctrl), 500 μM dibutyryl-cAMP (cAMP) for 6 h (n = 6) (left), or 1 μM rosiglitazone (Rosi) for 4 days (n = 6) (right).

(F) Immunoblot analyses for phosphorylation of PKA substrate and CREB in differentiated C2C12 cells expressing *Gabpa* in the presence of 2 mM Nic for indicated time or 500 μM dibutyryl-cAMP (cAMP) for 15 min. β-actin served as a loading control.

(G) qPCR analyses of *Chrna2*, *Ucp1*, and glucose metabolism gene expression in differentiated C2C12 cells expressing *Gabpa* following treatment with vehicle (Ctrl) or 2mM Nic for 6 h (n = 4).

(H) Intracellular L-lactate levels in differentiated C2C12 cells expressing *Gabpa* following treatment with vehicle (Ctrl) or 2 mM Nic for 6 h (n = 12).

(I) CHRNA2 agonist ACh (500 μM for 30 min)-induced oxygen consumption rate in differentiated C2C12 cells expressing empty vector or *Gabpa* under pro-adipogenic conditions (n = 10).

Data are presented as mean ± SEM. *p < 0.05, **p < 0.01, and ***p < 0.005 by an unpaired two sample Student's t test for two-group comparisons. See also Figure S5.

expressing C2C12 cells (Figures 5F and 5G). We further examined cellular glycolysis and OCR to test whether the activation of CHRNA2 signaling indeed stimulates glucose utilization and energy expenditure in differentiated *Gabpa*-expressing C2C12 cells. Both lactate levels and OCR were elevated when CHRNA2 signaling was activated by nicotine in the cultured g-beige adipocytes (Figures 5H and 5I). This indicated that functional CHRNA2 signaling can be induced by GABPα in a cell-autonomous fashion in g-beige fat. Conversely, it is worth noting that GABP has also been implicated in regulating the expression

levels of other AChRs, such as epsilon and gamma subunits at the neuromuscular junction in skeletal muscle (Briguet and Ruegg, 2000; O'Leary et al., 2007), suggesting an intimate cross-talk between this Ets-related transcription factor and acetylcholine signaling in general. These data collectively reveal an orchestrated regulation of these distinct subset of thermogenic cells through β-adrenergic-independent CHRNA2 signaling.

Since the rediscovery of thermogenic fat in human adults, research efforts have been directed toward identifying drug targets to activate thermogenic activity, increasing energy expenditure for weight loss and metabolic fitness. Agonists targeting the canonical regulatory pathway through β-adrenergic receptors have yet to be proven viable for clinical use, due to undesirable side effects including cardiovascular irregularities and elevated blood pressure in humans (Arch, 2011; Cypess et al., 2015). The β-adrenergic-independent signaling through CHRNA2 presents an alternative mechanism that circumvents the potential complications of sympathetic activation. It has been well documented that adrenergic signaling decreases in human adipose tissue with the onset of various illnesses, obesity, and aging (Faulds et al., 2003; Horowitz and Klein, 2000; Lönnqvist et al., 1990), conditions affecting people that would otherwise benefit the most from therapeutics that aim to improve metabolic health through activating adaptive thermogenesis. G-beige fat, the subpopulation of thermogenic fat cells that emerges in the absence of β-adrenergic signaling, represents a readily accessible therapeutic target in human subjects experiencing decreasing sympathetic tone and the onset of catecholamine resistance. The discovery that CHRNA2 plays a regulatory role in g-beige fat, reveals an attractive β-adrenergic-alternative therapeutic strategy in this rapidly evolving field.

STAR★METHODS

Detailed methods are provided in the online version of this paper and include the following:

- KEY RESOURCES TABLE
- RESOURCE AVAILABILITY
  - Lead Contact
  - Materials Availability
  - Data and Code Availability
- EXPERIMENTAL MODEL AND SUBJECT DETAILS
  - Mice
  - Cell Culture
- METHOD DETAILS
  - Metabolic Phenotyping
  - Genotyping
  - Calcium Imaging Assay
  - Gene Overexpression and Knockdown
  - Gene Expression Analysis
  - Immunoblotting
- MITOCHONDRIAL DNA CONTENT
  - Oil Red O
  - Intracellular Lactate levels
  - Cytochrome C Release
  - Tissue Histology
  - Citrate Synthase Activity
  - Respiration
- QUANTIFICATION AND STATISTICAL ANALYSIS

AUTHOR CONTRIBUTIONS

H.J., Y.M., Y.C., J.G., S.L., J. Wang, A.J.K., X.Q., and M.P.E. performed experiments; H.J., Y.M., X.Z.S.X., S.K., and J. Wu analyzed data; H.J., Y.M., A.J.K., and J. Wu wrote the manuscript; J. Wu oversaw the study.

DECLARATION OF INTERESTS

The authors declare no competing interests.

REFERENCES

Altshuler-Keylin, S., Shinoda, K., Hasegawa, Y., Ikeda, K., Hong, H., Kang, Q., Yang, Y., Perera, R.M., Debnath, J., and Kajimura, S. (2016). Beige adipocyte maintenance is regulated by autophagy-induced mitochondrial clearance. Cell Metab. 24, 402–419.

Anunciado-Koza, R., Ukropec, J., Koza, R.A., and Kozak, L.P. (2008). Inactivation of UCP1 and the glycerol phosphate cycle synergistically increases energy expenditure to resist diet-induced obesity. J. Biol. Chem. 283, 27688–27697.

Arch, J.R. (2011). Challenges in β(3)-adrenoceptor agonist drug development. Ther. Adv. Endocrinol. Metab. 2, 59–64.

Bachman, E.S., Dhillon, H., Zhang, C.Y., Cinti, S., Bianco, A.C., Kobilka, B.K., and Lowell, B.B. (2002). betaAR signaling required for diet-induced thermogenesis and obesity resistance. Science 297, 843–845.

Bertholet, A.M., Kazak, L., Chouchani, E.T., Bogaczyńska, M.G., Paranjpe, I., Wainwright, G.L., Bétourné, A., Kajimura, S., Spiegelman, B.M., and Kirichok, Y. (2017). Mitochondrial patch clamp of beige adipocytes reveals UCP1-positive and UCP1-negative cells both exhibiting futile creatine cycling. Cell Metab. 25, 811–822.e4.

Briguet, A., and Ruegg, M.A. (2000). The Ets transcription factor GABP is required for postsynaptic differentiation in vivo. J. Neurosci. 20, 5989–5996.

Cannon, B., and Nedergaard, J. (2004). Brown adipose tissue: function and physiological significance. Physiol. Rev. 84, 277–359.

Chen, Y., Ikeda, K., Yoneshiro, T., Scaramozza, A., Tajima, K., Wang, Q., Kim, K., Shinoda, K., Sponton, C.H., Brown, Z., et al. (2019). Thermal stress induces glycolytic beige fat formation via a myogenic state. Nature 565, 180–185.

Chondronikola, M., and Sidossis, L.S. (2019). Brown and beige fat: From molecules to physiology. Biochim. Biophys. Acta Mol. Cell Biol. Lipids 1864, 91–103.

Chruscinski, A.J., Rohrer, D.K., Schauble, E., Desai, K.H., Bernstein, D., and Kobilka, B.K. (1999). Targeted disruption of the beta2 adrenergic receptor gene. J. Biol. Chem. 274, 16694–16700.

Collins, S. (2011). beta-adrenoceptor Signaling Networks in Adipocytes for Recruiting Stored Fat and Energy Expenditure. Front. Endocrinol. 2, 102.

Developmental Cell
Article

CellPress

Cypess, A.M., Weiner, L.S., Roberts-Toler, C., Franquet Elía, E., Kessler, S.H., Kahn, P.A., English, J., Chatman, K., Trauger, S.A., Doria, A., and Kolodny, G.M. (2015). Activation of human brown adipose tissue by a β3-adrenergic receptor agonist. Cell Metab. *21*, 33–38.

de Jonge, L., and Bray, G.A. (1997). The thermic effect of food and obesity: a critical review. Obes. Res. *5*, 622–631.

Faulds, G., Rydén, M., Ek, I., Wahrenberg, H., and Arner, P. (2003). Mechanisms behind lipolytic catecholamine resistance of subcutaneous fat cells in the polycystic ovarian syndrome. J. Clin. Endocrinol. Metab. *88*, 2269–2273.

Feldmann, H.M., Golozoubova, V., Cannon, B., and Nedergaard, J. (2009). UCP1 ablation induces obesity and abolishes diet-induced thermogenesis in mice exempt from thermal stress by living at thermoneutrality. Cell Metab. *9*, 203–209.

Fernandes, G.W., Ueta, C.B., Fonseca, T.L., Gouveia, C.H., Lancellotti, C.L., Brum, P.C., Christoffolete, M.A., Bianco, A.C., and Ribeiro, M.O. (2014). Inactivation of the adrenergic receptor beta2 disrupts glucose homeostasis in mice. J. Endocrinol. *221*, 381–390.

Hibi, M., Oishi, S., Matsushita, M., Yoneshiro, T., Yamaguchi, T., Usui, C., Yasunaga, K., Katsuragi, Y., Kubota, K., Tanaka, S., and Saito, M. (2016). Brown adipose tissue is involved in diet-induced thermogenesis and whole-body fat utilization in healthy humans. Int. J. Obes. *40*, 1655–1661.

Horowitz, J.F., and Klein, S. (2000). Whole body and abdominal lipolytic sensitivity to epinephrine is suppressed in upper body obese women. Am. J. Physiol. Endocrinol. Metab. *278*, E1144–E1152.

Ikeda, K., Kang, Q., Yoneshiro, T., Camporez, J.P., Maki, H., Homma, M., Shinoda, K., Chen, Y., Lu, X., Maretich, P., et al. (2017). UCP1-independent signaling involving SERCA2b-mediated calcium cycling regulates beige fat thermogenesis and systemic glucose homeostasis. Nat. Med. *23*, 1454–1465.

Jun, H., Yu, H., Gong, J., Jiang, J., Qiao, X., Perkey, E., Kim, D.I., Emont, M.P., Zestos, A.G., Cho, J.S., et al. (2018). An immune-beige adipocyte communication via nicotinic acetylcholine receptor signaling. Nat. Med. *24*, 814–822.

Kazak, L., Chouchani, E.T., Jedrychowski, M.P., Erickson, B.K., Shinoda, K., Cohen, P., Vetrivelan, R., Lu, G.Z., Laznik-Bogoslavski, D., Hasenfuss, S.C., et al. (2015). A creatine-driven substrate cycle enhances energy expenditure and thermogenesis in beige fat. Cell *163*, 643–655.

Kazak, L., Chouchani, E.T., Lu, G.Z., Jedrychowski, M.P., Bare, C.J., Mina, A.I., Kumari, M., Zhang, S., Vuckovic, I., Laznik-Bogoslavski, D., et al.

(2017). Genetic depletion of adipocyte creatine metabolism inhibits diet-induced thermogenesis and drives obesity. Cell Metab *26*, 660–671.e3.

Kazak, L., Rahbani, J.F., Samborska, B., Lu, G.Z., Jedrychowski, M.P., Lajoie, M., Zhang, S., Ramsay, L.C., Dou, F.Y., Tenen, D., et al. (2019). Ablation of adipocyte creatine transport impairs thermogenesis and causes diet-induced obesity. Nat. Metab. *1*, 360–370.

Leibel, R.L., Rosenbaum, M., and Hirsch, J. (1995). Changes in energy expenditure resulting from altered body weight. N. Engl. J. Med. *332*, 621–628.

Lönnqvist, F., Nyberg, B., Wahrenberg, H., and Arner, P. (1990). Catecholamine-induced lipolysis in adipose tissue of the elderly. J. Clin. Invest. *85*, 1614–1621.

Marlatt, K.L., and Ravussin, E. (2017). Brown adipose tissue: an update on recent findings. Curr. Obes. Rep. *6*, 389–396.

O'Leary, D.A., Noakes, P.G., Lavidis, N.A., Kola, I., Hertzog, P.J., and Ristevski, S. (2007). Targeting of the ETS factor GABPalpha disrupts neuromuscular junction synaptic function. Mol. Cell. Biol. *27*, 3470–3480.

Roh, H.C., Tsai, L.T.Y., Shao, M., Tenen, D., Shen, Y., Kumari, M., Lyubetskaya, A., Jacobs, C., Dawes, B., Gupta, R.K., and Rosen, E.D. (2018). Warming induces significant reprogramming of beige, but not brown, adipocyte cellular identity. Cell Metab. *27*, 1121–1137.e5.

Rohrer, D.K., Desai, K.H., Jasper, J.R., Stevens, M.E., Regula, D.P., Jr., Barsh, G.S., Bernstein, D., and Kobilka, B.K. (1996). Targeted disruption of the mouse beta1-adrenergic receptor gene: developmental and cardiovascular effects. Proc. Natl. Acad. Sci. USA *93*, 7375–7380.

Rothwell, N.J., and Stock, M.J. (1979). A role for brown adipose tissue in diet-induced thermogenesis. Nature *281*, 31–35.

Susulic, V.S., Frederich, R.C., Lawitts, J., Tozzo, E., Kahn, B.B., Harper, M.E., Himms-Hagen, J., Flier, J.S., and Lowell, B.B. (1995). Targeted disruption of the beta 3-adrenergic receptor gene. J. Biol. Chem. *270*, 29483–29492.

Thomas, S.A., and Palmiter, R.D. (1997). Thermoregulatory and metabolic phenotypes of mice lacking noradrenaline and adrenaline. Nature *387*, 94–97.

Wang, Y., Paulo, E., Wu, D., Wu, Y., Huang, W., Chawla, A., and Wang, B. (2017). Adipocyte liver kinase b1 suppresses beige adipocyte renaissance through class IIa histone deacetylase 4. Diabetes *66*, 2952–2963.

Yu, H., Emont, M., Jun, H., and Wu, J. (2018). Isolation and differentiation of murine primary brown/beige preadipocytes. Methods Mol. Biol. *1773*, 273–282.

STAR★METHODS

KEY RESOURCES TABLE

REAGENT or RESOURCE	SOURCE	IDENTIFIER
Antibodies		
Rabbit polyclonal anti-UCP1	Abcam	Cat# ab10983; RRID: AB_2241462
Rabbit polyclonal anti-α-tubulin	Cell Signaling	Cat# 2144; RRID: AB_2210548
Total OXPHOS rodent antibody cocktail	Abcam	Cat# ab110413; RRID: AB_2629281
Rabbit monoclonal anti-phospho-CREB	Cell Signaling	Cat# 9198; RRID: AB_2561044
Rabbit monoclonal anti-CREB	Cell Signaling	Cat# 9197; RRID: AB_331277
Rabbit polyclonal anti-HSP90	Cell Signaling	Cat# 4874; RRID: AB_2121214
Rabbit polyclonal anti-phospho-PKA substrate	Cell Signaling	Cat# 9621; RRID: AB_330304
Rabbit monoclonal anti-COX IV	Cell Signaling	Cat# 4850; RRID: AB_2085424
Rabbit monoclonal anti-VDAC	Cell Signaling	Cat# 4661; RRID: AB_10557420
Rabbit monoclonal anti-β-actin	Cell Signaling	Cat# 8457; RRID: AB_10950489
Chemicals		
3-Isobutyl-1-methylxanthine	Sigma Aldrich	Cat# I7018
Acetylcholine chloride	Sigma Aldrich	Cat# A2661
Biotin	Sigma Aldrich	Cat# B4639
CL 316.243 hydrate	Sigma Aldrich	Cat# C5976
Dexamethasone	Sigma Aldrich	Cat# D4902
Dibutyryl-cAMP	Sigma Aldrich	Cat# D0260
D-pantothenic acid hemicalcium salt	Sigma Aldrich	Cat# P5155
Fura 2-AM	Sigma Aldrich	Cat# F0888
Insulin for cells	Sigma Aldrich	Cat# I5500
Insulin – Humulin R for ITT	Eli Lily	Cat# HI-210
Isoproterenol	Sigma Aldrich	Cat# I6504
Nicotine	Sigma Aldrich	Cat# N3876
Oligomycin A	Sigma Aldrich	Cat# 75351
Propranolol hydrochloride	Sigma Aldrich	Cat# PHR1308
Tri Reagent	Sigma Aldrich	Cat# 93289
Rosiglitazone	Cayman chemical	Cat# 71740
Recombinant human BMP4	R&D Systems	Cat# 3141-BP-010
Collagenase D	Roche	Cat# 11088882001
Dispase II	Roche	Cat# 04942078001
SYBR Green	Applied Biosystems	Cat# 4368708
M-MLV Reverse Transcriptase	Invitrogen	Cat# 28025021
Critical Commercial Assays		
Cytochrome c Release Assay Kit	Abcam	Cat# ab65311
Citrate Synthase Activity Assay Kit	Cayman chemical	Cat# 701040
L-Lactate Assay Kit	Cayman chemical	Cat# 1200011002
Experimental Models: Cell Lines		
C2C12 cells	ATCC	Cat# CRL-1772
Mouse primary inguinal preadipocytes	N/A	N/A
Human primary adipose stromal cells	Dr. Jeffrey M. Gimble	N/A
Experimental Models: Organisms/Strains		
Mouse: *Adiponectin-Cre*	The Jackson Laboratory	Cat# 010803
Mouse: *Myod1-Cre*^ERT2	The Jackson Laboratory	Cat# 025667

Developmental Cell
Article

CellPress

Continued

REAGENT or RESOURCE	SOURCE	IDENTIFIER
Mouse: *Ucp1* knockout	The Jackson Laboratory	Cat# 003124
Mouse: C57BL/6J	The Jackson Laboratory	Cat# 00664
Mouse: *Ucp1-Cre*	The Jackson Laboratory	Cat# 024679
Mouse: *Chrna2* knockout	The Jackson Laboratory	Cat# 005797
Mouse: β-less	Dr. Brad Lowell	N/A
Mouse: β1WT	Dr. Jun Wu	N/A
Mouse: β3WT	Dr. Jun Wu	N/A
Mouse: *Chrna2*fl/fl	Dr. Jun Wu	N/A
Oligonucleotides		
qPCR primers, see Table S1	Integrated DNA Technologies	N/A
Genotyping: *Chrna2* floxed 5' Fwd AGCACCAATCTGCGTTAATCTATG	Integrated DNA Technologies	N/A
Genotyping: *Chrna2* floxed 5' Rev ACTGTGAGATAGGGACAGAAAAGA	Integrated DNA Technologies	N/A
Genotyping: *Chrna2* floxed 3' Fwd CTGCCTTTTCATGCTGCACTCC	Integrated DNA Technologies	N/A
Genotyping: *Chrna2* floxed 3' Rev CCTCAGGGTCACCCAATCACAGA	Integrated DNA Technologies	N/A
Genotyping: *Adrb1* WT Fwd TCGCTACCAGAGTTTGCTGA	Integrated DNA Technologies	N/A
Genotyping: *Adrb1* WT Rev GGCACGTAGAAGGAGACGAC	Integrated DNA Technologies	N/A
Genotyping: *Adrb1* KO/*Adrb2* KO 2/*Adrb3* KO Fwd TCGCCTTCTTGACGAGTTCT	Integrated DNA Technologies	N/A
Genotyping: *Adrb1* KO Rev GCCTTCTTGACGAGTTCT	Integrated DNA Technologies	N/A
Genotyping: *Adrb2* WT/*Adrb2* KO 1 Fwd GAGCGACTACAAACCGTCAC	Integrated DNA Technologies	N/A
Genotyping: *Adrb2* WT Rev CAGCAAGTCTCCTCGGTGTA	Integrated DNA Technologies	N/A
Genotyping: *Adrb3* WT Rev GCATGTTGGAGGCAAAGGAA	Integrated DNA Technologies	N/A
Genotyping: *Adrb3* KO Rev GCTTAGCCACAACGAACACTC	Integrated DNA Technologies	N/A
Recombinant DNA		
MSCV-GFP	Dr. Jun Wu	N/A
MSCV-CRE	Dr. Jun Wu	N/A
Lentiviral vector for *Gabpa*	GeneCopoeia	Cat# EX-Mm02614-Lv120
Lentiviral shRNA clones 1 and 2 for *Gabpa*	GeneCopoeia	Cat# MSH027139-LVRU6GH
Lentiviral shRNA clones for scrambled control	GeneCopoeia	Cat# CSHCTR001-LVRU6GH
Software and Algorithms		
ImageJ	NIH	https://imagej.nih.gov/ij/
Excel	Microsoft	https://www.microsoft.com/
GraphPad Prism 8	GraphPad Software	https://www.graphpad.com/
MetaFluor software	Molecular Devices	https://www.moleculardevices.com/

RESOURCE AVAILABILITY

Lead Contact

Further information and requests for resources and reagents should be directed to and will be fulfilled by the Lead Contact, Jun Wu (wujunz@umich.edu).

Materials Availability

Further information and requests for resources and reagents should be directed to and will be fulfilled by the Lead Contact, Jun Wu (wujunz@umich.edu).

Data and Code Availability

This study did not generate any unique datasets or code.

EXPERIMENTAL MODEL AND SUBJECT DETAILS

Mice

All animal studies were conducted according to the protocol reviewed and approved by the Institutional Animal Care and Use Committee at the University of Michigan. All mice were housed under 12 h light/12 h dark cycle with a standard rodent chow diet (5L0D, PicoLab) unless otherwise indicated. The *Adiponectin-Cre* (Stock no. 010803), *Myod1-Cre*^ERT2 (Stock no. 025667), *Ucp1* knockout (Stock no. 003124), C57BL/6J (Stock no. 00664), *Ucp1-Cre* (Stock no. 024679) and *Chrna2* knockout mice (Stock no. 005797) were obtained from the Jackson Laboratory. β-less mice were provided by Brad Lowell (Beth Israel Deaconess Medical Center, Boston). β1WT and β3WT mice were generated by crossing β-less animals with 129SVE mice purchased from Taconic Farms Inc (model no. 129 SVE). *Chrna2*^fl/fl mice were generated using CRISPR/Cas9-mediated homology-directed insertion of LoxP sites flanking exon 3, by the Michigan Diabetes Research Center Molecular Genetics Core at the University of Michigan. Designed sgRNAs were validated to ensure that they cut the target sites accurately within the *Chrna2* locus. Zygotes injected with the sgRNA and Cas9 were cultured until the blastocyst stage by the University of Michigan Transgenic Animal Core. The target region of sgRNAs on Chrna2 locus was amplified by PCR using genomic DNA extracted from the lysed blastocysts and verified through sequencing. Cas9, sgRNA and oligonucleotide containing LoxP sites were injected into fertilized mouse eggs and transferred to pseudo-pregnant recipient mice for gestation. Insertion of LoxP sites was confirmed by PCR amplification of the target region in tail genomic DNA from potential founders. To generate fat-specific *Chrna2* KO mice (*Chrna2*-adKO), *Chrna2*^fl/fl mice were crossed with *Adiponectin-Cre* mice. Thermogenic fat-specific *Chrna2* KO mice (*Ucp1-Cre*;*Chrna2*^fl/fl) were generated by crossing *Chrna2*^fl/fl mice with *Ucp1-Cre* mice. CL 316,243-injected (1 mg/kg/day for 3 days) *Ucp1-Cre*;*Chrna2*^fl/fl and littermate *Chrna2*^fl/fl control mice were housed at room temperature for 21 days and then subjected to cold exposure at 10°C for 2 weeks. The CL 316,243 pretreatment and recovery for 3 weeks will ensure *Cre*-mediated deletion occurs in beige adipocytes in IWAT and thermogenic gene expression goes back to basal level as previously reported (Altshuler-Keylin et al., 2016; Roh et al., 2018; Wang et al., 2017).

Age-matched adult *Chrna2*-adKO and littermate control mice (5-10 weeks old) were used for cold and acute or chronic HFD experiments. For cold exposure studies, mice were singly housed in pre-chilled cages in a 10°C environmental chamber for 2 weeks. For acute HFD experiments, C57BL/6J and *Ucp1* KO mice were maintained on either a chow diet or a HFD consisting of 60% of calories from fat (D12491, Research Diets) for 3 days or 10 days at room temperature (23°C). To study the effects of acute HFD at thermoneutrality, mice were housed at 30°C for 3 weeks on a chow diet and then received either a chow diet or a HFD for 3 days. For chronic HFD studies, mice were singly housed and fed HFD (45% of calories from fat; D12451, Research Diets) for 11 weeks at room temperature. Over this period, body weight and food intake were measured weekly.

To recruit glycolytic beige fat in IWAT of WT C57BL/6J or *Chrna2* KO mice, animals were given intraperitoneal injections of β-blocker (propranolol hydrochloride) at a dose of 25 mg/kg (body weight) per day, for a period of 5 days at room temperature. Mice were then exposed to cold (15°C) or kept at room temperature for an additional 5 days under the same treatment. Mice genetically lacking β-AR signaling including β-less, β1WT and β3WT were housed at room temperature or cold for 5 days.

Cell Culture

The isolation, culture and differentiation of primary SVF from adipose depots were performed as described previously (Yu et al., 2018). Briefly, fat tissues were dissected, minced and digested in collagenase D (1.5 U/mL) and dispase II (2.4 U/mL) solution supplemented with 10 mM CaCl$_2$ for 15 to 20 minutes in a 37 °C water bath with agitation. Digested tissues were filtered through a 100 μm cell strainer and centrifuged at 300–500 × *g* for 5 minutes to pellet cells. The floating mature adipocytes were collected when needed for gene expression analyses. The cell pellet was resuspended and passed through a 40 μm cell strainer and centrifuged as above. The SVF was collected when needed for gene expression analyses. The cell pellet was resuspended with culture medium (DMEM/F12 GlutaMAX containing 15 % FBS and penicillin/streptomycin) and plated onto a collagen-coated 10 cm cell culture dish. For adipocyte differentiation, confluent cultures of cells were exposed to induction medium (DMEM/F-12 GlutaMAX supplemented with 10% FBS, penicillin/streptomycin, 0.5 μg/mL insulin, 5 μM dexamethasone, 1 μM rosiglitazone and 0.5 mM IBMX). Two days after induction, cells were cultured in maintenance medium containing 10% FBS, penicillin-streptomycin and 0.5 μg/mL insulin until they were ready for analyses. For adenovirus transduction of differentiated primary preadipocytes, adipocytes were incubated with adenoviral CRE recombinase or GFP in maintenance medium for 24 hours. After replacing of the medium, the cells were cultured for an additional 48 hours.

Human adipose precursor cells from subcutaneous adipose tissue were obtained from healthy adult liposuction patients (a gift from Dr. Jeffrey M. Gimble at Tulane University). All specimens were collected under the protocols reviewed and approved by the Western Institutional Review Board (Puyallup, WA) or the University of Michigan Medical School Institutional Review Board (IRBMED). Cells were grown in MesenPRO RS medium supplemented with penicillin/streptomycin and differentiated in DMEM/F12 GlutaMAX supplemented

Developmental Cell
Article

CellPress

with 10% FBS, dexamethasone (5 μM), insulin (0.5 μg/mL), IBMX (0.5 mM), rosiglitazone (5 μM), biotin (33 μM), pantothenic acid (17 μM), and BMP4 (20 ng/ml) for 3 days. On day 4, cells were cultured in maintenance medium (DMEM/F12 GlutaMAX containing 10% FBS, 0.5 μg/mL insulin, 5 μM dexamethasone, 33 μM biotin, and 17 μM pantothenic acid) until they were fully differentiated. HEK293T cells and C2C12 cell lines were obtained from ATCC. HEK293T cells were grown in DMEM supplemented with 10% FBS. C2C12 cells and the immortalized *Myod+* progenitors isolated from IWAT of *Myod1-Cre*^ERT2 reporter mice after injection of β-blocker for 5 days were cultured and differentiated as previously described (Chen et al., 2019).

METHOD DETAILS

Metabolic Phenotyping

Fasting (4 hours) blood glucose levels at the basal condition were determined using the OneTouch Ultra Glucometer (Lifescan) in tail blood from mice. For glucose tolerance test (GTT), mice fed HFD for 9 weeks were fasted for 16 hours and received an intraperitoneal injection of 1.5 g/kg glucose. Insulin tolerance test (ITT) were performed after 10 weeks on HFD. Mice were fasted for 4 hours and 1 U/kg insulin (Eli Lilly) was administered by intraperitoneal injection. Glucose levels were determined from tail blood at 15, 30, 60, 90, and 120 minutes after glucose or insulin injection. The area under the curve (AUC) from GTT or ITT was analyzed using Prism 8. Chronic cold-exposed animals were subjected to nuclear magnetic resonance (NMR) analysis for body composition measurement (fat and lean mass). Whole-body energy expenditure (VO_2 and VCO_2), glucose oxidation and locomotor activity (at the x axis and y axis) of cold-exposed mice were monitored at 10°C for 48 hours using a Comprehensive Laboratory Monitoring System (Columbus Instruments) at the University of Michigan Animal Phenotyping Core. Core body temperature was measured using a RET-3 rectal probe (World Precision Instruments).

Genotyping

All knockout and *Cre*-transgenic mice obtained from the Jackson Laboratory were genotyped using PCR according to the protocol provided by the Jackson Laboratory. Genotyping of the *Chrna2* floxed allele was performed by PCR using the following primers designed to detect the specific insertion sites of LoxP on 5' and 3' ends: 5' end forward (F), 5'-AGCACCAATCTGCGTTAATCTATG-3'; 5' end reverse (R), 5'-ACTGTGAGATAGGGACAGAAAAGA-3' and 3' end F, 5'-CTGCCTTTTCATGCTGCACTCC-3'; 3' end R, 5'-CCTCAGGGTCACCCAATCACAGA-3'. To generate β1WT and β3WT mice by crossing β-less mice with 129SVE mice, primers to detect wild-type (WT) or knockout (KO) alleles in *Adrb1*, *Adrb2* or *Adrb3* were designed based on the gene targeting strategies described previously (Chruscinski et al., 1999; Rohrer et al., 1996; Susulic et al., 1995): *Adrb1* WT F, 5'-TCGCTACC AGAGTTTGCTGA-3'; *Adrb1* WT R, 5'-GGCACGTAGAAGGAGACGAC-3'; *Adrb1* KO F/*Adrb2* KO F2/*Adrb3* KO F, 5'-TC GCCTTCTTGACGAGTTCT-3'; *Adrb1* KO R, 5'-TGGCTCTCTACACCTTGGAC-3'; *Adrb2* WT F/*Adrb2* KO F1, 5'-GAGCGACT ACAAACCGTCAC-3'; *Adrb2* WT R, 5'-CAGCAAGTCTCCTCGGTGTA-3' and *Adrb3* WT F, 5'-CGCCGAGACTACAGACCATA-3'; *Adrb3* WT R, 5'-GCATGTTGGAGGCAAAGGAA-3'; *Adrb3* KO R, 5'-GCTTAGCCACAACGAACACTC-3'. Of note, the primer for *Adrb1* KO F/*Adrb2* KO F2/*Adrb3* KO F was designed targeting to the inserted Neo cassette. The Neo cassette was reversed in *Adrb2* KO animals and thus the KO alleles were genotyped using two forward primers.

Calcium Imaging Assay

SVF isolated from mouse IWAT was seeded on collagen-coated glass bottom culture dishes (Mat Tek Corporation) and induced to differentiate. Fully differentiated adipocytes were loaded with 10 μM of Fura 2-AM at 37°C. After 30 minutes they were washed twice with standard Tyrode's solution (135 mM NaCl, 4 mM KCl, 10 mM glucose, 10 mM HEPES, 2 mM $CaCl_2$, and 1 mM $MgCl_2$, pH 7.4) at room temperature. Calcium assays were performed using an Olympus IX73 invert microscope under a 40× objective. Fluorescence signals were recorded upon sequential excitation with 340 nm followed by 380 nm with an ORCA-Flash 4.0 sCMOS camera (Hammatsu Inc.) with MetaFluor software (Molecular Devices Inc.). After establishing a baseline 340/380 nm ratio, the CHRNA2 agonist (500 μM nicotine or 100 μM acetylcholine) was perfused onto the cells.

Gene Overexpression and Knockdown

The lentiviral vector for *Gabpa* overexpression was purchased from GeneCopoeia (EX-Mm02614-Lv120). Lentiviral shRNA clones 1 and 2 for *Gabpa* were also obtained from GeneCopoeia (MSH027139-LVRU6GH for mouse *Gabpa* and CSHCTR001-LVRU6GH for a scrambled control). For lentivirus production, HEK293T packaging cells were transfected with 10 μg lentiviral vectors using the calcium phosphate method. After 48 hours of incubation, the viral supernatant was collected and filtered. C2C12 cells and primary inguinal adipocytes were incubated overnight with the viral supernatant supplemented with 10 μg/mL polybrene. Puromycin at a dose of 2 μg/mL or hygromycin at a dose of 200 μg/mL were used for selecting the stable-expressing cells.

Gene Expression Analysis

Total RNA from tissues and cultured cells was extracted using the Tri Reagent method (Sigma Aldrich). For quantitative real-time PCR (qPCR) analysis, an equal amount of RNA was used to synthesize cDNA according to the manufacturer's protocol for M-MLV Reverse Transcriptase (Life Technologies). qPCR reactions were performed in a 384-well format using Power SYBR Green (Thermo Fisher Scientific). Relative mRNA levels were calculated using the $\Delta\Delta C_T$ method and normalized to *Tbp*, *36B4 or Atp5e*. Primer sequences can be found in Table S1.

Immunoblotting

Total protein from mouse adipose tissue was prepared in ice-cold lysis buffer (50 mM Tris-HCl, pH 7.5, 1% Triton X-100, 1% sodium deoxycholate, 0.1% SDS, 150 mM NaCl, 1 mM phenylmethylsulfonyl fluoride) supplemented with a protease inhibitor cocktail (Roche) and phosphatase inhibitors (10 mM NaF, 60 mM β-glycerolphosphate, pH 7.5, 2 mM sodium orthovanadate, 10 mM sodium pyrophosphate). Proteins were subjected to SDS-PAGE then transferred onto polyvinylidene difluoride (PVDF) membranes. The membranes were probed with following antibodies: UCP1 (Abcam, ab10983), Total OXPHOS Rodent Antibody Cocktail (Abcam, ab110413), COXIV (Cell Signaling, 4850), VDAC (Cell Signaling, 4661), HSP90 (Cell Signaling, 4874), phospho-PKA substrate[S/T] (Cell Signaling, 9621), phospho-CREB[S133] (Cell Signaling, 9198), CREB (Cell Signaling, 9197), β-actin (Cell Signaling, 8457) and α-tubulin (Cell Signaling, 2144).

MITOCHONDRIAL DNA CONTENT

Total DNA was extracted from IWAT of cold-exposed animals using Tri Reagent (Sigma Aldrich) according to the provided protocol. The amounts of nuclear *Lpl* and mitochondrial *Nd1* in genomic DNA were determined using qPCR analysis. The expression levels of mitochondrial *Nd1* were normalized with those of nuclear *Lpl* to estimate mitochondrial DNA copy numbers.

Oil Red O

Control vector- or *Gabpa*-expressing C2C12 cells were differentiated under pro-adipogenic conditions. Cells were fixed in 10% formalin for at least an hour, and then washed with 60% isopropanol. Subsequently, cells were dried, stained with Oil Red O solution for 10 minutes and then washed with H_2O. Images were obtained with a Leica DMIRB microscope.

Intracellular Lactate levels

Intracellular lactate was extracted and measured in differentiated primary β-less inguinal preadipocytes or *Gabpa*-expressing C2C12 cells using L-Lactate Assay Kit (Cayman) according to the provided protocol.

Cytochrome C Release

Cytochrome c protein abundance was determined in purified mitochondria and cytosol organelles of IWAT from β-less or β-blocker-injected WT mice using Cytochrome c Release Assay Kit according to manufacturer's instructions (Abcam). Total mitochondrial protein mass was analyzed in the isolated mitochondria fraction.

Tissue Histology

Adipose tissue depots were harvested and fixed overnight in 10% formalin at 4°C. Routine paraffin-embedding and hematoxylin-eosin (H&E) staining were performed by the University of Michigan Comprehensive Cancer Center Research Histology and Immuno-peroxidase Laboratory. Images were obtained with a LEICA DM2000. H&E stained images of IWAT from HFD-fed mice (n = 3 per genotype) were subjected to analysis of adipocyte size using ImageJ software (Adiposoft).

Citrate Synthase Activity

Citrate synthase activity of mouse inguinal adipose tissue was measured with a citrate synthase activity assay kit according to manufacturer's instructions (Cayman Chemical). The homogenates of IWAT were prepared using extraction buffer (50 mM Tris-HCl, 1 mM $MgCl_2$, 100 mM KCl, 250 mM sucrose and 30 mM 2-mercaptoethanol) and centrifuged at 1,000 x *g* for 15 minutes at 4 °C. The supernatants were subjected to analyses of citrate synthase activity and protein levels for normalization.

Respiration

Freshly harvested inguinal fat was weighed and minced in respiration buffer (2.5 mM glucose, 2.5 mM sodium pyruvate, 1 mM malate, 120 mM NaCl, 4.5 mM KCl, 0.7 mM Na_2HPO_4, 1.5 mM NaH_2PO_4 and 0.5 mM $MgCl_2$, pH 7.4). Oxygen consumption was recorded at each stage (basal or uncoupled with 4 mg/mL oligomycin) using a Clark electrode (Strathkelvin Instruments). Basal oxygen consumption rate in primary inguinal *Ucp1* KO or β-less adipocytes was measured in the culture medium. Oxygen consumption in C2C12 cells was determined using the Seahorse XFe24 Analyzer (Agilent) as described previously (Chen et al., 2019).

QUANTIFICATION AND STATISTICAL ANALYSIS

All results are presented as means ± standard error of the mean (SEM) and graphed using Prism 8 software (GraphPad). Data are representative of 2–4 independent experiments. Sample sizes are biological replicates and were chosen based on preliminary data or previously published reports. Data for whole-body energy expenditure in the cold exposure study were analyzed by using analysis of covariance with body weight as a covariate. Statistical analyses were performed using Microsoft Excel or Prism software. Data were analyzed by an unpaired two sample Student's t-test for two-group comparisons or a one-way analysis of variance (ANOVA) for multiple comparisons involving one independent variable.